Dalton Transactions

PAPER

View Article Online
View Journal | View Issue

Cite this: *Dalton Trans.*, 2015, **44**, 13282

Unusual coordination state of cobalt ions in zeolites modified by aluminum chloride

M. I. Shilina,*[a] G. Yu. Vasilevskii,[a] T. N. Rostovshchikova[a] and V. Yu. Murzin[b]

Received 30th April 2015,
Accepted 11th June 2015

DOI: 10.1039/c5dt01640a

www.rsc.org/dalton

Co- and Al-modified zeolites (Al–Co–ZSM-5) were prepared by solid-state ion exchange with cobalt acetate or chloride, followed by $AlCl_3$ immobilization from anhydrous toluene solution. Based on data from XRD, X-ray absorption (XANES/EXAFS), X-ray photoelectron spectroscopy and DRIFT spectral studies of adsorbed probe molecules (carbon monoxide, ethane), a new cobalt electronic state, bonded with surface aluminum atoms through oxygen and chlorine atoms, arises on the surface of Al–Co–ZSM-5. A new band at 2192 cm^{-1} appears in the DRIFT spectrum, shifted to lower frequencies compared to CO complexes with isolated Co^{2+} cations (2205 cm^{-1}). Spectral data of the ethane adsorption (new strong bands in the range of 2740–2770 cm^{-1}) prove the existence of specific centers of alkane activation on coordinately unsaturated cobalt cations, resulting in the interaction with aluminum chloride.

Introduction

Zeolites are widely used as heterogeneous catalysts for hydrocarbon conversion because of their unique channel structures, thermal stability, acidity, shape-selective properties and great selectivity for cation exchange. The design of single-site heterogeneous catalysts based on zeolites, and understanding their mechanisms of action, have growing interest and practical importance. An unusual method of hydrocarbon activation *via* metal–alkyl compounds has been proposed for zeolites modified with Zn and Ga.[1,2] Moreover metal–alkyl intermediates were observed in gas–phase reactions of hydrocarbons with Co^+, Fe^+, Ni^+, and Mo^+ ions.[3,4] It was found recently that high-silica zeolites modified with cobalt salts and aluminum chloride were one order of magnitude more active and selective for paraffin conversion in the liquid phase at medium temperatures (130–190 °C) than the parent support.[5] The synergistic action of Lewis acids and transition metal salts is also known for the catalytic isomerization of alkanes, the alkylation of unsaturated and aromatic compounds, and in the cracking of heavy paraffins.[6–9] This effect is commonly attributed to the formation of complexes that are more acidic than the initial Lewis acid.[9–11] This is favorable for the formation of carbocations, which are key intermediates in the conversion of hydrocarbons in the presence of acid catalysts, including the hydrogen forms of zeolites.[11–13] However, in some cases transition metal cations themselves can interact directly with hydrocarbons, but only at elevated temperatures of >500 °C. In accordance with low-temperature *in situ* IR spectroscopy and DFT calculations,[14–18] C_7–C_{10} alkanes may be activated even at low temperatures of 170–230 K on transition metal (Co, Ni *etc.*) halide–aluminum halide complexes formed in the reaction medium. In this case the reaction does not yield cracking products and takes place *via* the intermediate formation of dimetal alkyl complexes, not *via* the carbocation mechanism that is commonly accepted for acid catalysis. The introduction of transition metal cations into the zeolite may increase the probability of alkane activation *via* the alkyl route.

This work aims to establish the structural features and reasons for the synergistic action of transition metal and Lewis acid additives in catalysis by the Al–Co-modified ZSM-5 zeolite, taking CO and ethane as test molecules for analysis of adsorption properties. The modified Al–Co–ZSM-5 zeolite was prepared using cobalt acetate or chloride as precursors in solid-state ion exchange, followed by $AlCl_3$ immobilization from anhydrous toluene solution. The Co coordination geometry and electronic state were investigated by X-ray diffraction (XRD), X-ray photoelectron spectroscopy (XPS) and X-ray absorption spectroscopy (EXAFS and XANES). New adsorption and catalytic sites resulting from the introduction of both modifiers into the zeolite were detected by diffuse reflectance infrared Fourier transform (DRIFT) spectroscopy, including the carbon monoxide and ethane adsorption technique.

Experimental

Materials

Zeolite NH_4–ZSM-5 (Zeolyst Co.) with SiO_2/Al_2O_3 = 55 and a specific surface area of 425 m^2 g^{-1} was pressed into pellets,

[a]*Department of Chemistry, Lomonosov Moscow State University, 1-3, Leninskiye Gory, GSP-1 Moscow, 119991, Russia. E-mail: mish@kinet.chem.msu.ru*
[b]*National Research Centre "Kurchatov Institute", 1, Akademika Kurchatova pl., Moscow, 123182, Russia*

which were then ground. Granules 0.4–0.8 mm in diameter were used in experiments. The hydrogen form of the zeolite was obtained by calcination of the initial zeolite at 500–520 °C for 8 h in flowing air. Aluminum chloride (99.99%, Aldrich) was used as received. All manipulations involving this compound were performed in a dry argon atmosphere or in a vacuum. Cobalt chloride $CoCl_2 \cdot 6H_2O$ (analytical grade, Acros Organics) was used in the form of a crystalline hydrate or was dehydrated prior to use by heat treatment in a vacuum at 150 °C for 3–4 h. Cobalt acetate $Co(CH_3COO)_2 \cdot 4H_2O$ (reagent grade, Irea2000) was used as received. Toluene was used freshly distilled from P_2O_5. Argon (special-purity grade) was additionally dried by passing through columns packed with calcined zeolite NaX, $CaCl_2$ and P_2O_5.

Zeolite modification

Zeolite Co–ZSM-5 was prepared by solid-state ion exchange between H–ZSM-5 and cobalt acetate or chloride. A salt–zeolite mixture was held at 450–500 °C in flowing argon for 6 h (heating rate of 5 °C min^{-1}). The resulting material was washed with distilled water and was dried at room temperature for 1 day and then at 120 °C for 8 h. Thereafter, the zeolite was calcined at 450 °C for 3 h in flowing air. Herein, Co–ZSM-5 catalysts are identified as Co–Z-X, where X indicates the cobalt precursor – acetate (ac) or chloride (cl).

Al–Co–ZSM-5 samples were synthesized by treatment with anhydrous $AlCl_3$: a mixture of anhydrous aluminum chloride with Co-modified zeolite (Co–ZSM-5) in toluene was boiled in flowing dry argon. Hydrogen chloride formed during the reaction (1)

$$n(\text{–OH}) + AlCl_3 \rightarrow (\text{–O–})nAlCl_{3-n} + n\text{HCl} \quad (1)$$

was absorbed with the 0.1 M KOH aqueous solution. After completion of the reaction (1.5–2 h), the product was decanted and washed with hot toluene in flowing argon to remove the residual aluminum chloride, and the solvent was removed by heating the product under vacuum (200 °C, 3 h).

The resulting zeolites were stored and manipulated in an argon-filled dry box.

Zeolite characterization

The composition of the samples was analyzed by ICP-OES on an iCAP 6300 Duo Thermo Electron, and the results are shown in Table 1. The corresponding Co contents are denoted in the catalyst identification column, for example, Co–Z-0.9-cl corresponds to a Co content of 0.9 wt% in the catalyst.

The amount of hydrogen chloride evolved in reaction (1) was measured by acid–base titration and is shown in Table 1. According to ICP data, the molar ratio of evolved HCl to aluminum introduced into the zeolite was (1.0–1.4) : 1, which indicates that the aluminum chloride was anchored as $(\text{–O–})AlCl_2$ and $(\text{–O–})_2AlCl$.

IR spectroscopy

DRIFT and transmission IR spectra were recorded on an Infralum FT-801 (Lyumeks-Sibir') Fourier spectrometer fitted with a diffuse reflectance attachment. DRIFT spectra were recorded in the 900–6000 cm^{-1} range (4 cm^{-1} resolution, 128 scans) at room temperature. Granules of the modified zeolite or initial support (0.4–0.6 mm) were placed in a quartz tube with a CaF_2 optical window and were heat treated at 200 °C for 2 h and at 400 °C for 3 h in a vacuum (residual pressure of 0.01 Pa or below). CO was adsorbed on heat-treated samples at room temperature, with the gas pressure in the optical reactor varied from 0.005 to 1.5 kPa.

Transmission IR spectroscopic measurements were carried out with a resolution of 4 cm^{-1}, and the number of scans was equal to 64. The samples were prepared by compressing the solids in order to obtain self-supporting pellets. They were mounted on a transportable infrared cell with KBr windows and an external oven. The pretreatment was performed at 450 °C under a dynamic vacuum of 1.3×10^{-2} Pa for 3 h.

XAS and XRD

X-ray absorption spectroscopy and X-ray diffraction analysis were conducted at the Structural Materials Science end-station of the National Research Centre "Kurchatov Institute" (Moscow, Russia).[19] Diffraction patterns were registered in the Debye–Scherrer transmission geometry. Photosensitive Imaging Plate (FujiFilm) detectors were used and the exposure time was 15 min. Phase identification was made with the help of the PDF-2 database.[20] The wavelength was calibrated using a Zr foil standard and fixed at the Zr absorption K-edge (0.68886 Å or 17998 eV). The sample-to-detector distance and tilts were determined using a Si powder standard (NIST SRM 640c).

Table 1 Synthesis and characterization of modified zeolites

Sample	Precursor	Co, wt%	Co/Al_{sum} [a]	Co/Al_F [a]	DE, %[b]	$AlCl_x$[c], mmol g^{-1}	HCl[d], mmol g^{-1}
Co–Z-0.9-cl	$CoCl_2$	0.92	0.27	0.27	55	—	
Co–Z-0.9-ac	$Co(CH_3COO)_2 \cdot 4H_2O$	0.91	0.27	0.27	54	—	
Co–Z-2.1-ac	$Co(CH_3COO)_2 \cdot 4H_2O$	2.1	0.62	0.62	125	—	
Al–Co–Z-0.9-cl	$CoCl_2$	0.92	0.14	0.27	55	0.55	0.75
Al–Co–Z-0.9-ac	$Co(CH_3COO)_2 \cdot 4H_2O$	0.91	0.13	0.27	54	0.61	0.65
Al–Co–Z-2.1-ac	$Co(CH_3COO)_2 \cdot 4H_2O$	2.1	0.28	0.62	125	0.72	0.73

[a] Co/Al atomic ratio, calculated from ICP data, where Al_{sum} = total Al in the sample and Al_F = amount of Al in the framework. [b] DE (degree of exchange) = $200Co/Al_F$. [c] Calculated from ICP data as $Al_{sum} - Al_F$. [d] The amount of hydrogen chloride evolved in reaction (1).

The absorption spectra at the Co K-edge were measured in fluorescence mode by means of an ionization chamber filled with air and a silicon (single crystal) avalanche photodiode detector. A Si(111) channel-cut monochromator was used. The third harmonics rejection was made by pressing on the top crystal plane with a piezo-drive within intrinsic elasticity limits. Taking into account the fluorescence mode, errors due to higher harmonics contamination were expected to be negligible. The spectra were processed with the IFEFFIT software package,[21] whereas the phases and amplitudes of photoelectron scattering used to refine local structure parameters were calculated with the FEFF program.[22] The interval of electron wave numbers (k) in the procedure of model refinement was 2.0–10.0 $Å^{-1}$. The interval of the fit in R-space was set to 1.2–3.5 Å. The determination error was about 10–20% for coordination numbers and about 1–2% for interatomic distances. $CoCl_2$, $CoCl_2 \cdot 6H_2O$ and $Co(CH_3COO)_2 \cdot 4H_2O$ were used as reference compounds. The passive electron reduction factor S0 and the energy shift ΔE were fixed at values of 0.85 and 4.0 eV, respectively. XAS measurements were carried out at ambient pressure.

XPS

The X-ray photoelectron spectra were collected using an Axis Ultra DLD (Kratos, UK) spectrometer using monochromatic AlK_α radiation at an X-ray unit power of 150 W. Crushed granules were used for these studies. The spectra were measured at transmission energies of 160 and 40 eV for a survey spectrum and the spectra of individual lines, respectively. The spectral regions corresponding to Co 2p, O 1s, C 1s, Si 2p, Si 2s and Al 2p core levels were recorded for each sample. The BE reference value was C 1s = 284.8 eV. The peak areas were determined by integration employing a Shirley-type background. Peaks were considered to be a mixture of Gaussian and Lorentzian functions in a 70 : 30 ratio. In order to remove the effect of sample charging, the spectra were measured with the use of a neutralizer.

Results and discussion

IR spectroscopy

The modification of H–ZSM-5 with cobalt and aluminum salts alters the hydroxyl cover of the zeolite. The FTIR spectra of the parent H–ZSM-5 zeolite and the cobalt-containing samples prepared from cobalt chloride (Co–Z-0.9-cl) and additionally modified with aluminum chloride (Al–Co–Z-0.9-cl) are compared in Fig. 1. All the spectra were normalized to the intensity of the lattice vibrations at 2000 and 1880 cm^{-1}. The spectrum of H–ZSM-5 shows absorption bands at 3744 and 3613 cm^{-1} and a broad band at 3300–3500 cm^{-1}. According to the data,[23–30] these bands are due to O–H vibrations in silanol (Si–OH) and bridging (Si–OH–Al) hydroxyl groups in the free and hydrogen-bonded states.

As one can see from Fig. 1, the introduction of cobalt reduces the integral intensities of all the main vibrational

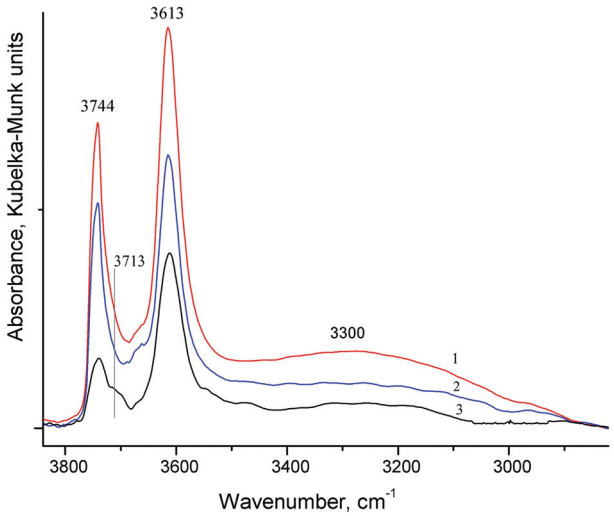

Fig. 1 FTIR spectra of zeolites in the region of O–H stretching vibrations: (1) H–ZSM-5, (2) Co–Z-0.9-cl and (3) Al–Co–Z-0.9-cl.

bands of O–H in H–ZSM-5: the broad band at 3300–3500 cm^{-1}, which is due to associated bridging groups, and the bands of free Si–OH–Al (3613 cm^{-1}) and silanol groups (3744 cm^{-1}). Subsequent treatment of Co–Z-cl with aluminum chloride results in a further decrease of the intensity of both OH vibration bands. Therefore, the protons of different hydroxyl groups participate in ion exchange with aluminum chloride. The greatest decrease in relative intensity is observed for the ν(OH) band of the Si–OH groups at 3744 cm^{-1}. At the same time, new weak bands at 3713 cm^{-1} appear in the spectrum. The observed changes likely arise from the formation of (–O–)$AlCl_x$ (x = 1 or 2) fragments bonded to silicon or aluminum atoms on the support surface *via* reaction (1).[5,31] In particular, the 3713 cm^{-1} band is assignable to vibrations of terminal Si–OH groups whose oxygen atom interacts with the extraframework Al atom of a (–O–)$AlCl_x$ fragment anchored to adjacent Si or Al atoms. Similar coordination of terminal Si–OH groups with extraframework aluminum atoms is indicated in the spectrum of H–ZSM-5.[27,28] In addition, it is possible that direct contact occurs between cations of cobalt and aluminum. DRIFT spectra of the Co–Z-ac and Al–Co–Z-ac were discussed in an earlier publication.[5] The impact of zeolite modification using cobalt acetate and aluminum chloride on the hydroxyl cover of the support was very similar to that observed using cobalt chloride.

DRIFT spectra of adsorbed carbon monoxide

Co–Z samples. Fig. 2 and 3 present the DRIFT spectra of the Co-modified zeolites (ac, cl) in the region of the CO stretching mode, recorded after carbon monoxide adsorption at room temperature (RT) and at a pressure of 0.7 kPa and below. CO adsorption on the acid sites of H–ZSM-5, as we have shown previously,[5] was observed in the DRIFT spectra at RT only at pressures above 0.7 kPa, including a band at 2169 cm^{-1} due to

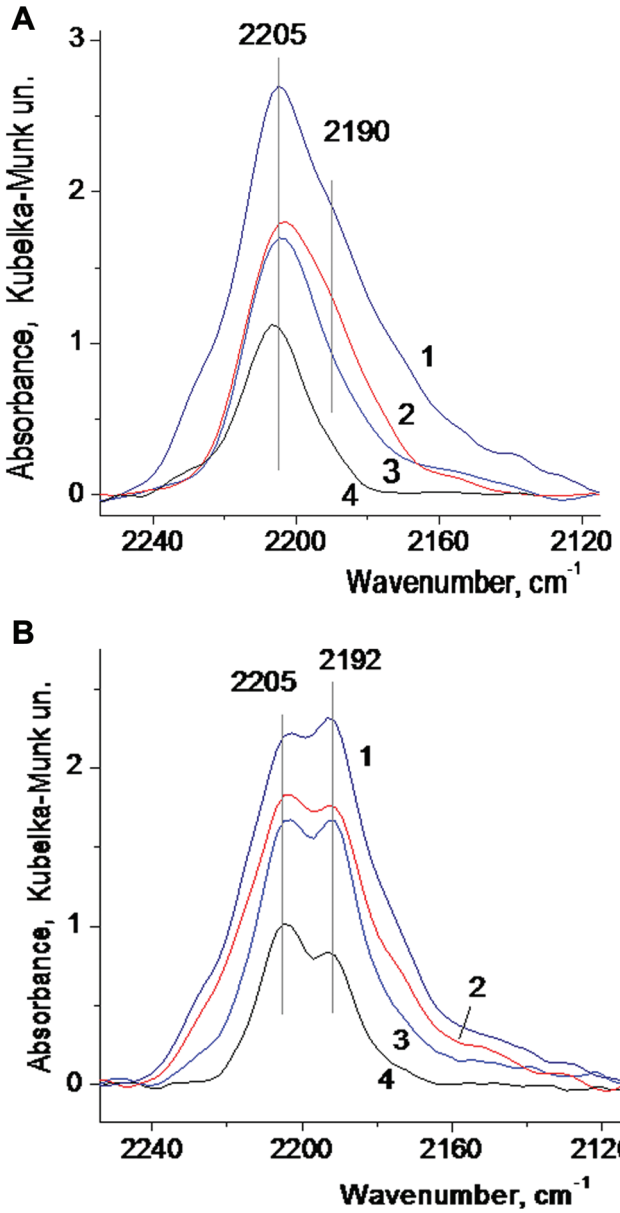

Fig. 2 DRIFT spectra of carbon monoxide adsorbed at RT and at equilibrium pressure of 0.7 kPa (1), and vacuumed to pressure 0.1 kPa (2,3) and 0.005 kPa (4), on (A) Co–Z-0.9-ac (1,3,4) and Co–Z-0.9-cl (2) and (B) Al–Co–Z-0.9-ac (1,3,4) and Al–Co–Z-0.9-cl (2). The spectra are background corrected.

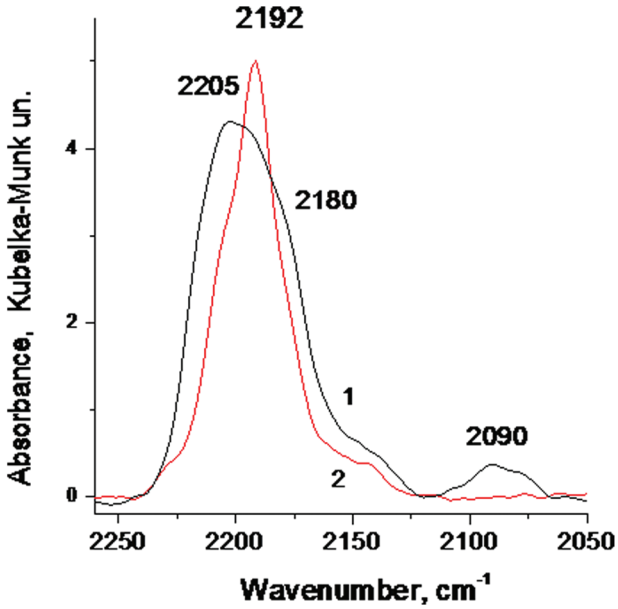

Fig. 3 DRIFT spectra of carbon monoxide adsorbed at RT on (1) Co–Z-2.1-ac and (2) Al–Co–Z-2.1-ac at equilibrium pressure of 0.7 kPa. The spectra are background corrected.

the H complexes of carbon monoxide with bridging protons of acidic Si–OH–Al groups,[23–26] and weak bands at 2189 and 2221 cm^{-1} that indicate the presence of Lewis acid sites.[24,30,32]

The spectra of CO adsorbed on the Co-modified zeolites (Fig. 2 and 3) at equilibrium CO pressure of 0.7 kPa and below indicate the formation of stronger adsorption sites on their surfaces, and the CO bands in this region can be ascribed to Co species. It is known that the frequency of adsorbed CO ν(CO) depends on the valence and coordination states of the cations related to their ability to accept σ-donation (increasing ν(CO)) and to donate π-orbitals of CO (decreasing ν(CO)).[24] The spectra in Fig. 2(A) for the samples Co–Z-09 (-ac and -cl) with degree of exchange (DE) < 100% (and Co/Al < 0.5) show a strong wide band at about 2200 cm^{-1}, which is a superposition of absorption bands at 2205 and 2190 cm^{-1}. The 2205 cm^{-1} band is due to the complexes of CO with isolated Co^{2+} cations in exchange positions.[33–35] The shoulder of the lower frequency band may be due to $[Co–O–Co]^{2+}$ oxide-like structures,[33,34] $CoOH^{+}$ ions, or phyllosilicates.[35] At the same time the band at 2205 cm^{-1} may be related to the carbonyl complex with Co^{3+} ions,[33,36,37] arising after calcination of Co-containing zeolite at high temperatures in a stream of air. Low-temperature CO adsorption studies on Co_3O_4 showed a strong band at 2195 cm^{-1},[38] while the CO adsorption on CoO usually occurs at 2175–2180 cm^{-1}.[24,34]

As one can see from the comparison of spectra 2 and 3 in Fig. 2(A), for the samples Co–Z-0.9-ac and -cl (DE < 100%) the Co precursor slightly affects the ratio of intensities of the bands at 2205 and 2190 cm^{-1}. Only the contribution of oxide-like structures $[Co–O–Co]^{2+}$ (with the band at 2190 cm^{-1}) weakly increases when cobalt chloride was used as precursor.

In contrast, the proportion of Co in oxide-like forms increases with increasing cobalt content in the zeolite, as one can see in Fig. 3, where the spectra of CO adsorbed on the sample Co–Z-2.1-ac (DE > 100%) are presented for example. Spectrum 1 in Fig. 3 shows a strong wide band at about 2200 cm^{-1}, which is a superposition of absorption bands at 2205, 2190 and 2180 cm^{-1}. With the bands for Co^{2+} cations (2205 cm^{-1}) and oxide-like structures $[Co–O–Co]^{2+}$ (2190 cm^{-1}), new low frequency bands at ~2180 cm^{-1} associated most likely with oxide structures including oligomeric

oxides and even small cobalt oxide nanoparticles[24,33,34] appeared. Reduction of the frequency of adsorbed CO in the series (Co^{2+} in exchange positions > Co^{2+} in "oxide-like clusters" > Co^{2+} in bulk CoO) is due to the decrease of electron-acceptor properties of the adsorption sites of Co^{2+}.

In addition, low oxidation states of cobalt may be present on the surface of Co-containing zeolites in the course of the CO adsorption at RT, which is manifested in the IR spectra by the carbonyl complexes detected below 2100 cm^{-1}. For such complexes ν(CO) is lowered compared to $\nu(CO)_{gas}$ because the CO molecule is partially bound to adsorption sites by the use of occupied d-orbitals when $d \rightarrow \pi^*$ donation takes place. As one can see in Fig. 3, new small bands at ~2090 cm^{-1} arise in the spectra of adsorbed CO on the Co–Z-2.1-ac, which are related to CO complexes with Co^{+} ions.[39,40] Similar cobalt reduction by carbon monoxide on the surface of Co zeolites is associated mainly with the reduction of $[Co–O–Co]^{2+}$ ions.[40]

According to DRIFT spectra of adsorbed CO, in addition to isolated Co^{2+} ions and $[Co–O–Co]^{2+}$ ions, cobalt oxide particles as Co_3O_4 or CoO may also be present on the surface of modified zeolites, especially at DE > 100%. Indeed, oxide-like particles, as will be shown below using XPS and X-ray spectroscopy, are present on the surface of prepared samples.

Al–Co–Z samples. Fig. 2(B) and 3 show the spectral variations in the DRIFT spectra of adsorbed CO resulting after treatment of Co-modified zeolites (Co–Z-0.9-ac and -cl and Co–Z-2.1-ac) with anhydrous $AlCl_3$. From comparison of the data in Fig. 2(A) and (B) one can see that a new band at 2192 cm^{-1} appears in Al–Co–Z-0.9, which is shifted to lower frequencies relative to the band of the complexes with isolated Co^{2+} ions (2205 cm^{-1}). There is no strong influence of the initial Co state in zeolites modified by cobalt acetate or chloride, as seen from the spectra 2 and 3 (Fig. 2(B)). It should be noted that there is no such absorption band in the spectra of parent H–ZSM-5 zeolite modified only by $AlCl_3$ (Al–Z) without the Co introduction.[5] Thus, the spectra of the cobalt carbonyl complexes (Fig. 2 and 3) indicate that the introduction of aluminum chloride generates new coordination states of the transition metal.

In comparing the spectra of Co–Z and Al–Co–Z for various Co contents (Fig. 2(A) and (B) for Co 0.9 wt% and spectra 1 and 2 in Fig. 3 for Co 2.1 wt%), we note that the increase in the intensity of the new band at 2192 cm^{-1} in the spectra of all samples Al–Co–Z is accompanied a decrease in the intensity of the band at 2205 cm^{-1}, which indicates a lowering the proportion of the isolated Co^{2+} ions in the total transition metal content after the aluminum chloride introduction on the Co–Z surface.

The closeness of the observed vibration bands for the CO adsorbed on oxide-like clusters in parent Co–Z (at 2190 cm^{-1}) and the new cobalt species in the Al–Co–Z (at 2192 cm^{-1}) makes it difficult to estimate a possible role of the $[Co–O–Co]^{2+}$ species on the Co–Z surface in the reaction with the anhydrous aluminum chloride. However, this evaluation may be obtained from the data of Co^{2+} ion reduction at RT. As one can see in Fig. 3, low frequency bands (near 2000–2100 cm^{-1}) corresponding, as noted above, to a low oxidation state of cobalt,[39,40] are absent in the spectrum of Al–Co–Z-2.1-ac, unlike in that of Co–Z-2.1-ac. This indicates a decrease of $[Co–O–Co]^{2+}$ ion proportion or a change in the structure of these ions in the Al–Co–Z after $AlCl_3$ treatment of the parent Co–Z sample, because these particles are most susceptible to reduction after exposure of samples to CO at RT.[40]

By this means, the DRIFT spectra of adsorbed CO showed that the introduction of aluminum chloride on the surface of the Co zeolite gives rise to new coordination states of the transition metal, in which the cobalt atoms are apparently coordinated with aluminum atoms through chlorine or oxygen atoms. According to ref. 41, similar uncommon transition metal states were observed in Fe–ZSM-5 treated with trimethylaluminium vapor under anhydrous conditions. The IR spectrum of adsorbed NO exhibited new bands due to Fe–O–Al structures that resulted from the interaction of iron cations with the introduced extraframework aluminum atoms.

DRIFT spectra of adsorbed ethane

To understand the role of these new sites in alkane activation, the adsorption of ethane on H–, Co– and Al–Co–Z was studied. Fig. 4 presents the spectra of the Co-containing zeolites in the region of C–H stretching bands, after adsorption of ethane at room temperature. The spectra of adsorbed ethane on the hydrogen form of ZSM-5 are very similar to those obtained previously[42,43] and contain three well-resolved and one unresolved C–H stretching bands. These can be assigned as follows (gas-phase frequencies[44] in parentheses): 2974 cm^{-1}, ν_7 (IR 2994 cm^{-1}); 2941 cm^{-1}, ν_{10} (Raman 2963 cm^{-1}); 2920 cm^{-1}, ν_5 (IR 2954 cm^{-1}); 2878 cm^{-1}, ν_1 (Raman 2899 cm^{-1}). Upon lowering the ethane pressure, all of the bands decreased in frequency in parallel and were completely eliminated by evacuation at room temperature. Subsequent adsorption of ethane regenerated the initial spectrum. This indicates weak and reversible adsorption of ethane by the hydrogen form of the zeolite.

As follows from Fig. 4(A), similar DRIFT bands were also observed after ethane adsorption by the cobalt-modified H–ZSM-5. However, in addition to the narrow bands at 2828, 2880, 2917, 2946 and 2982 cm^{-1}, DRIFT spectra of Co–Z-0.9 also contained a very strongly low-frequency shifted band with a maximum at 2755 cm^{-1}. Upon lowering the ethane pressure, the intensity of this broad band did not change very much, while those of the narrow bands decreased. Therefore, the overall spectrum of adsorbed ethane corresponds to a superposition of the bands from two different forms of adsorption. The narrow high-frequency bands belong to the weakly adsorbed species, while the broad low-frequency shifted band belongs to the stronger form of molecular adsorption.

The form of specific ethane adsorption has been observed previously on various bivalent cation (Ca, Mg, Zn *etc.*)-modified zeolites.[42,43] It has been demonstrated that the adsorption of light alkanes by cationic forms of various zeolites results in a variation of the distribution of the relative intensities of the absorption bands, which strongly depends both on the nature

of the cations and on the zeolite framework. It was also shown that the most strongly perturbed and polarized vibrations are the initially fully symmetric C–H stretching vibrations, which are directly connected with the chemical activation of adsorbed molecules. The greatest red shift of the C–H band was observed for C_2H_6 adsorption on Zn–ZSM-5.[43]

As one can see from Fig. 4(B), similar DRIFT bands were also observed for the Al–Co–Z-0.9-ac zeolite after ethane adsorption. However here, unlike the spectra of Co–Z-0.9-ac (Fig. 4(A)), the broad low-frequency shifted band belonging to the stronger form of molecular adsorption is composed of two overlapping bands at 2772 and 2743 cm^{-1}. Upon lowering the ethane pressure, the intensity of these broad bands did not change very much while that of the narrow bands at >2800 cm^{-1} decreased. The occurrence of two new bands attributed to a stronger form of molecular ethane adsorption also indicates the appearance of a new state of cobalt on the surface of the Co–ZSM-5 zeolite after the introduction of aluminum chloride that very likely plays a key role in alkane activation.

XRD

Fig. 5 presents the XRD patterns of the Co–Z-0.9-ac and Co–Z-0.9-cl samples prepared from cobalt acetate and chloride, and their changes after the introduction of aluminum chloride (Al–Co–Z-0.9-ac and Al–Co–Z-0.9-cl, respectively). According to XRD analysis, all the samples contain a crystalline H–ZSM-5 zeolite phase. A further detailed examination of the patterns using a high-energy X-ray source (around 17 keV) reveals reflexes that can be designated as a poorly crystallized Co_3O_4 spinel phase, most likely nanoparticles. The size of these nanoparticles should not extend several nanometers. The samples of both Co zeolites, which were obtained only from cobalt acetate and chloride, have the more crystallized spinel phase, while in the samples treated with aluminum chloride this phase looks more dispersed. Note that in contrast to this work, no other phase than the crystal phase of zeolite has been found at low (~1 wt%) Co composition by using a lower-energy X-ray source.[5,45]

XAS

The shape and position of the Co K-edge X-ray absorption near edge structure (XANES) provides information on the electronic structure and the local coordination geometry of the absorbing Co atom.[35,45–48] Fig. 6(A) presents the XANES spectra of the samples Co–Z-0.9 and Al–Co–Z-0.9 (-ac and -cl) and several cobalt compounds ($CoCl_2$, $Co(CH_3COO)_2{\cdot}4H_2O$ and $CoCl_2{\cdot}6H_2O$) measured under ambient conditions and serving as references. For reference compounds containing only Co(II) sites, the energy threshold appears at around 7720 eV, as seen in ref. 45 & 47. The energy threshold of the mixed-valence Co(II)/Co(III) reference compound Co_3O_4 is at 7723 eV.[47] XANES spectra of Co–Z-0.9-cl and Co–Z-0.9-ac (Fig. 6) show that in both samples cobalt has the mixed Co^{2+} and Co^{3+} state, and their energy threshold appears at around 7722 eV. They cannot be related to a pure cobalt chloride or oxide based on the

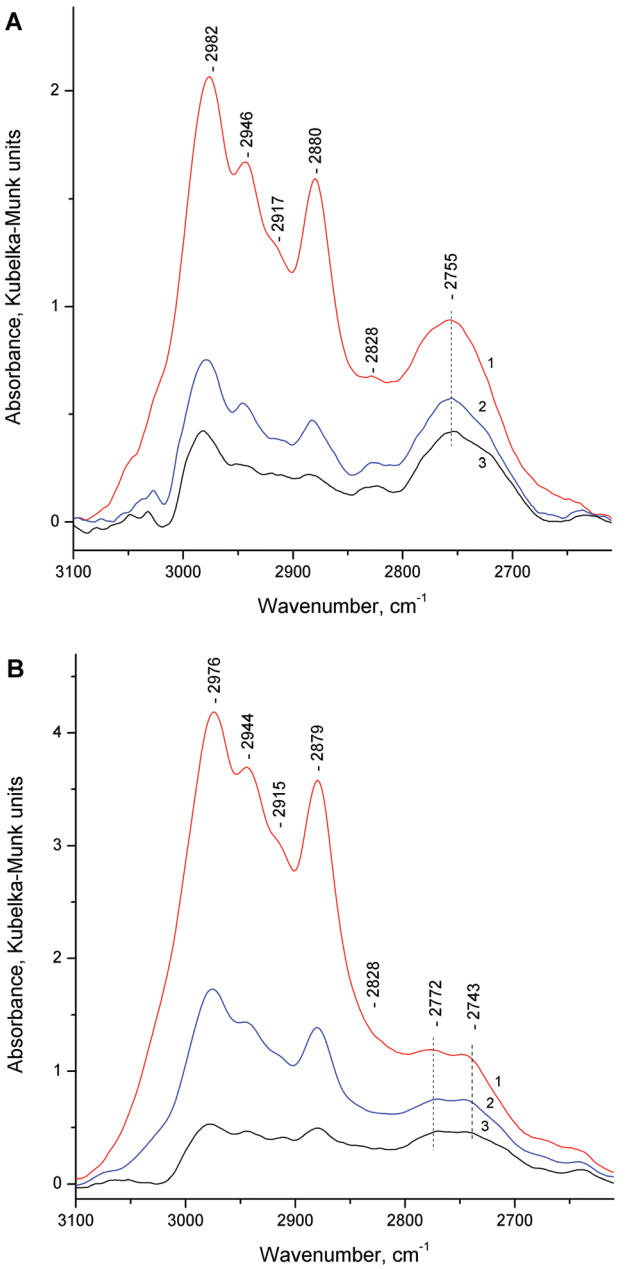

Fig. 4 DRIFT spectra of ethane adsorbed at RT on Co–Z-0.9-ac at various equilibrium pressures: (1) 0.6, (2) 0.3, (3) 0.2 kPa (A) and on Al–Co-Z-0.9-ac at various equilibrium pressures: (1) 1.3, (2) 0.6, (3) 0.3 kPa (B). The spectra are background corrected.

spectra for reference compounds and the spectra for various Co-containing spinel structures.[47] Samples of both Co–Z (-ac and -cl) have similar XANES spectra and this can be attributed to the mixture of Co ions in the spinel structure, and Co ions having a hydroxide shell that is close to cobalt in exchange positions in ZSM-5.[35,45,48–51]

The XANES spectra of the samples Al–Co–Z-0.9 (-ac and -cl) (Fig. 6(A), curves c and d) show that the treatment of the original Co–Z zeolites with anhydrous $AlCl_3$ induces changes in

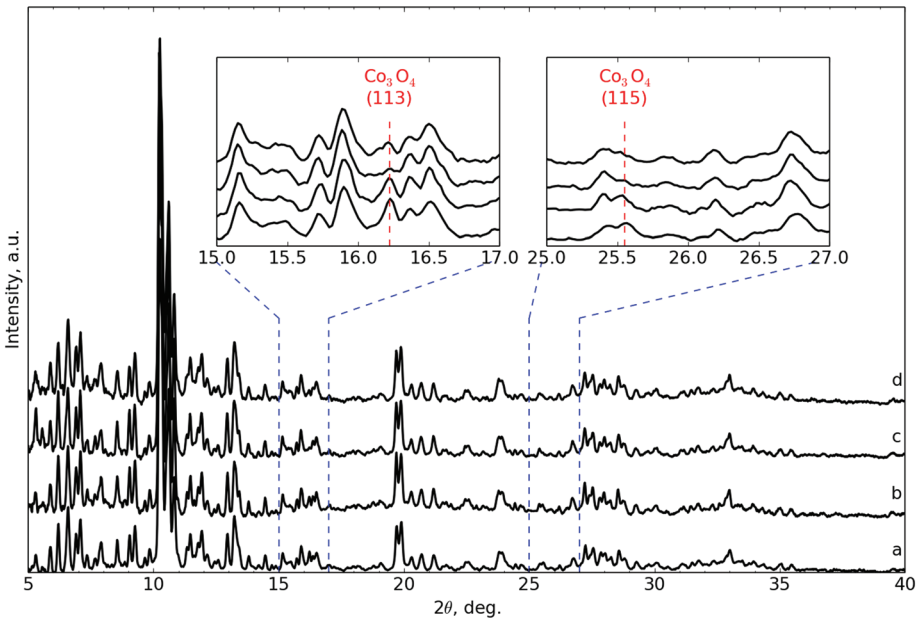

Fig. 5 XRD patterns of samples: (a) Co–Z-0.9-cl, (b) Co–Z-0.9-ac, (c) Al–Co–Z-0.9-cl and (d) Al–Co–Z-0.9-ac.

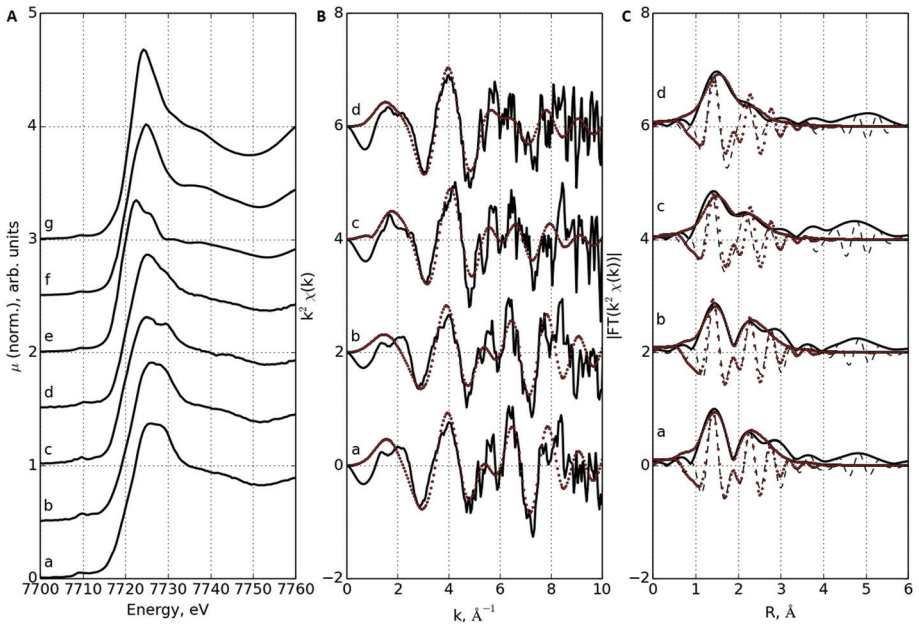

Fig. 6 K-edge XANES (left, A), k^2-weighted EXAFS functions (center, B) and Fourier transforms of k^2-weighted EXAFS functions (right, C, magnitudes are shown as solid black lines, imaginary parts are shown as dashed black lines) for samples: (a) Co–Z-0.9-cl, (b) Co–Z-0.9-ac, (c) Al–Co–Z-0.9-cl, and (d) Al–Co–Z-0.9-ac. $CoCl_2$ (e), $CoCl_2{\cdot}6H_2O$ (f) and $Co(CH_3COO)_2{\cdot}4H_2O$ (g) were used as reference compounds. Fits are presented as red dots.

the white line intensity, edge position, and oscillatory shape, suggesting that there are some changes in the Co coordination sphere. Samples of Al–Co–Z probably have some chlorine atoms adjacent to the cobalt atoms, in addition to some of the former Co coordination states. This can be deduced from the fact that XANES curves of the Al–Co–Z (-ac and -cl) bifurcate at the "white" line (see Fig. 6(A)).

EXAFS (extended X-ray absorption fine structure spectroscopy) analysis gives a clearer picture of the cobalt coordination and interatomic distances, since EXAFS signals mainly result from the interaction between an absorbing atom and nearby surrounding atoms.[46,48–51] Fig. 6(B) and (C) show the Co K-edge k^2-weighted EXAFS functions and their Fourier transforms for the samples Co–Z-0.9 and Al–Co–Z-0.9. In the

Fourier transforms of the EXAFS functions for the Co–Z (-cl and -ac) (Fig. 6(C), curves a and b) one can find three distinct coordination spheres, which can be assigned to one Co–O and two Co–Co environments. Results of the modeling of coordination numbers, interatomic distances and Debye–Waller parameters are presented in Table 2. In both samples, the first coordination sphere of the cobalt ions can be fitted with an octahedral environment of oxygen. The distances are in a good agreement with the spinel Co_3O_4 particles, but the coordination numbers for Co–Co contributions are definitely very low. This may correspond to small Co_3O_4 nanoparticles. The Co–Si and Co–Al paths were not included in the fit due to a lower contribution of Si and Al compared to Co in EXAFS. The first Co–O sphere could also include extra or intraframework Co that is not in the spinel nanoparticles and corresponds to Co^{2+} ions without any detectable second neighbours, represented as "intraframework ions", since no distinction can be made between poorly organized $(CoO_x)_n$ oligomers or truly isolated Co^{2+} ions. EXAFS spectra of these "intraframework ions" were observed for Co–ZSM-5 prepared by aqueous ion exchange from cobalt nitrate.[45,48]

As one can see from the Fourier transforms of the EXAFS functions for the Al–Co–Z (-cl and -ac) shown in Fig. 6C, curves c and d and from the data of Table 2, the treatment of the Co–Z samples with aluminum chloride leads to lower Co coordination numbers for Co–O and spinel environments in the model. Moreover, the Co–Cl contribution should be added to the fit. The coordination number is rather low but still this contribution cannot be neglected. Thus, the introduction of aluminum chloride on the surface of Co–Z results both in the higher dispersion of cobalt oxide phases and reduction of the proportion of cobalt atoms located in a spinel structure of Co_3O_4. In addition, chlorine atoms appear close to the transition metal, possibly as Co–Cl–Al structures. Such structures must be very sensitive to moisture as aluminum chloride itself easily hydrolyzes in air. Therefore, it was interesting to test whether the cobalt coordination environment in the Al–Co–Z could change after exposure to an air atmosphere. It should be noted that the previously mentioned XAS spectra (Fig. 6) were collected in an inert atmosphere, including sample preparation as well as spectra recording.

Fig. 7 shows a comparison of the EXAFS data obtained for the initial Al–Co–Z-0.9 (-cl and -ac) samples and after exposure to air atmosphere (marked with an asterisk). It can be seen that after contact with atmospheric moisture (Fig. 7, spectra b and d) the intensities of the bands assigned to the backscattering from the chlorine atoms coordinated to the cobalt ion (2.0 Å uncorrected) decrease whereas the intensities of the band assigned to backscattering from Co–O increase. Results of modeling are presented in Table 2. At the same time, the spectra of the initial Co–Z-0.9 (-cl and -ac) sample remained substantially unaltered after similar moisture contact (not shown).

Thus, in accordance with EXAFS and XANES studies, a chlorine atom is in the first coordination sphere of the cobalt ions at the distance of 2.36 Å in the Al–Co–Z samples regardless of the precursor. This value is characteristic for bridged Co–Cl bonds in the various $CoCl_2$ complexes with aluminum chloride, in which the bond length lies in the range of 2.33–2.50 Å depending on the structure.[15,16,52]

XPS

The Co 2p photoemission spectra of Co–Z-2.1-ac and Al–Co–Z-2.1-ac are shown in Fig. 8 in comparison with the spectrum of $CoCl_2$ serving as a reference. The Co $2p_{3/2}$ peaks and Co $2p_{1/2}$ peaks for Co–Z-2.1-ac appearing as broad bands in the regions 780–782 and 795–798 eV respectively indicate the

Table 2 Parameters obtained from the modeling of EXAFS functions for the Co–Z and Al–Co–Z samples recorded in an inert atmosphere. Samples marked with an asterisk (*) were recorded after storage in air

Sample	Path	N	R (Å)	σ^2 (Å^2)
Co–Z-0.9-cl	Co–O	5.5(5)	1.99(2)	0.0109(37)
	Co–Co	2.4(3)	2.88(3)	0.0057(22)
	Co–Co	2.6(4)	3.28(3)	0.0057(22)
Co–Z-0.9-ac	Co–O	5.5(5)	1.98(2)	0.0137(41)
	Co–Co	1.9(3)	2.87(3)	0.0056(21)
	Co–Co	2.1(4)	3.32(3)	0.0056(21)
Al–Co-0.9-cl	Co–O	4.4(5)	1.92(4)	0.0101(49)
	Co–Co	0.7(2)	2.78(5)	0.0058(28)
	Co–Co	2.1(3)	3.31(6)	0.0058(28)
	Co–Cl	1.1(2)	2.37(4)	0.0055(29)
Al–Co–Z-0.9-ac	Co–O	4.1(5)	1.96(4)	0.0100(49)
	Co–Co	1.0(2)	2.85(5)	0.0060(29)
	Co–Co	1.0(2)	3.32(6)	0.0060(29)
	Co–Cl	1.4(2)	2.36(5)	0.0057(31)
Al–Co-0.9-cl*	Co–O	4.7(5)	1.99(4)	0.0066(49)
	Co–Co	2.1(2)	2.83(5)	0.0067(28)
	Co–Co	0.9(3)	3.35(6)	0.0067(28)
	Co–Cl	0.8(2)	2.36(4)	0.0037(29)
Al–Co–Z-0.9-ac*	Co–O	4.5(5)	2.0(4)	0.0055(49)
	Co–Co	2.4(2)	2.84(5)	0.0070(29)
	Co–Co	1.1(2)	3.32(6)	0.0070(29)
	Co–Cl	1.0(2)	2.36(5)	0.0034(31)

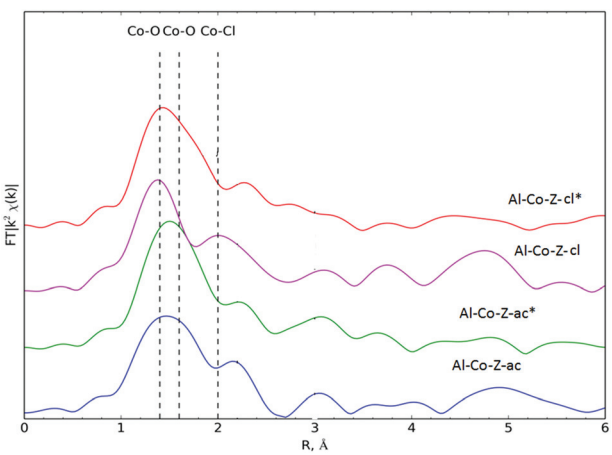

Fig. 7 Fourier transforms of k^2-weighted EXAFS functions for samples: Al–Co–Z-0.9-cl and Al–Co–Z-0.9-ac, obtained for the initial samples and after exposure to an air atmosphere (marked with an asterisk).

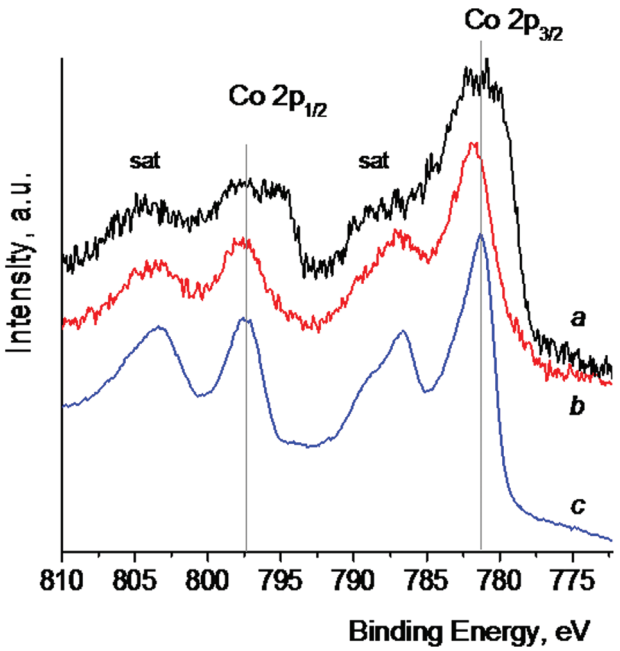

Fig. 8 Co 2p X-ray photoemission spectra of the samples (a) Co–Z-2.1-ac, (b) Al–Co–Z-2.1-ac and (c) $CoCl_2$. Samples for analysis were prepared in a dry box under Ar.

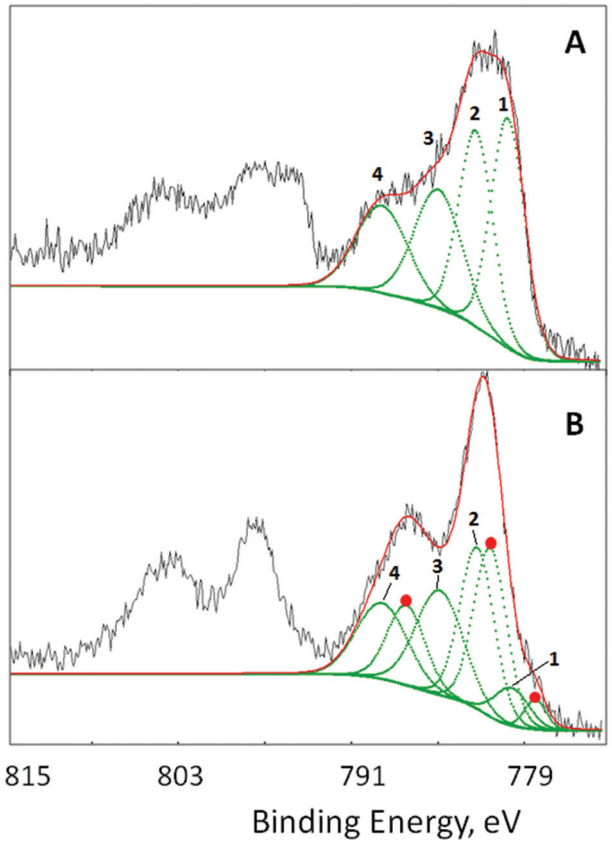

Fig. 9 Peak fitting analysis of Co 2p signals of XPS for samples (A) Co–Z-2.1-ac and (B) Al–Co–Z-2.1-ac. Peaks 1 and 2 with their corresponding satellites (peaks 3 and 4) are assigned to oxide or/and oxide similar particles and Co^{2+} ions respectively. The peaks marked with an asterisk are new after the separation of peaks 1–4 found for the spectrum of the sample Co–Z-2.1-ac.

presence of Co in more than one form. In addition to these spin-orbital peaks, satellites for $2p_{3/2}$ and $2p_{1/2}$ are also observed at 787 and 804 eV, respectively, confirming that cobalt is mainly present in the Co(II) oxidation state.[53–56]

Fig. 9(A) and Table 3 show the results of a peak-fitting analysis performed for the spectrum of the sample Co–Z-2.1-ac for the decomposition of the $2p_{3/2}$ main peak into a Co^{2+} peak at 782.3 ± 0.1 eV and a peak for the various oxides/silicate adspecies at 780.6 ± 0.1 eV, along with the decomposition of the satellite peak (spin-orbital splitting) into two peaks.

The component peak with a binding energy (BE) of 782.3 eV (accompanied by a "shake up" satellite line at 788.9 eV) can be associated with the Co $2p_{3/2}$ level of Co^{2+} ions in ion-exchange positions of the zeolite.[54–56] An additional component at a BE of 779.9 and a satellite peak at 788.9 eV can be attributed to Co oxide (most probably to CoO and/or Co_3O_4).[53]

As one can see from the comparison of XPS data for Co–Z-2.1-ac and Al–Co–Z-2.1-ac in Fig. 8, treatment of the Co–Z with $AlCl_3$ modifies the spectral parameters of the Co $2p_{3/2}$ and Co $2p_{1/2}$ peaks. The signals become narrower, and the corresponding binding energies (781.7 and 797.8 eV respectively) differ from the BEs of peaks 1 and 2 (see Fig. 9(A)).

The decomposition spectrum of the Al–Co–Z-2.1-ac was measured taking into account the fact that Co species existing in only the Co-modified zeolite may still remain after the $AlCl_3$ treatment. By this means the same parameters for bands 1–4 (binding energy, width-to-height ratio, Gaussian/Lorenzian ratio) as for the spectrum of the Co–Z-2.1-ac sample (Fig. 9(A)) were used for fitting the spectrum of the Al–Co–Z-2.1-ac sample. The results are summarized in Fig. 9 (B) and Table 3. These data show that the contents both of cobalt ions in exchange positions and in the various oxide or oxide-like structures are reduced. This reduction is most essential for oxide structures (BE 780.9 eV). At the same time new states of cobalt come into view on the surface of the modified Al–Co–Z-2.1-ac zeolite, which are marked in Fig. 9(B) with the circle.

This correlates with the above DRIFT spectra (see Fig. 2 and 3) of the adsorbed CO, which indicate a decrease of the proportion of the isolated Co^{2+} ions and of the $[Co–O–Co]^{2+}$ species in the total transition metal content after treatment of the Co–Z surface with anhydrous aluminum chloride.

The binding energy of the new main Co $2p_{3/2}$ peak (781.4 eV) of Al–Co–Z-2.1-ac is close to the BE of one of the main peaks of $CoCl_2$ (Peak 1, Table 3 and Fig. 10) that should indicate the creation of a Co–Cl bond in the sample Al–Co–Z-2.1-ac. These results are in a good agreement with the data from EXAFS and XANES studies (see Table 2). It should be noted that the second signal with a higher BE of Co $2p_{3/2}$ (at 783.5 eV) of $CoCl_2$ is not observed in spectrum of Al–Co–Z-2.1-ac. This may be related to the formation of bridged (but not

Table 3 Co $2p_{3/2}$ spectral fitting parameters: binding energy (eV) and percentage of total area[a]

Compound	Peak 1a[b], eV(%)	Peak 1, eV (%)	Peak 2a[b], eV (%)	Peak 2, eV (%)	Peak 3, eV (%)	Peak 4a[b], eV(%)	Peak 4, eV (%)
Co–Z-2.1-ac		779.9 (31.7)		782.3 (27.1)	784.9 (23.0)		788.9 (18.2)
Al–Co–Z-2.1-ac	**778.2** (2.7)	779.9 (5.3)	**781.4** (22.5)	782.3 (22.3)	784.9 (19.8)	**787.2** (12.10)	788.9 (15.4)
$CoCl_2$		781.3 (42.9)		783.5 (19.6)	786.6 (24.1)		789.1 (13.3)

[a] Fitting for Al–Co–Z-ac was realized assuming fitting parameters (binding energy (eV) and FWHM), which were found for the spectrum of Co–Z-ac. [b] New peaks according to the spectrum of Co–Z-ac (they are in bold typeface).

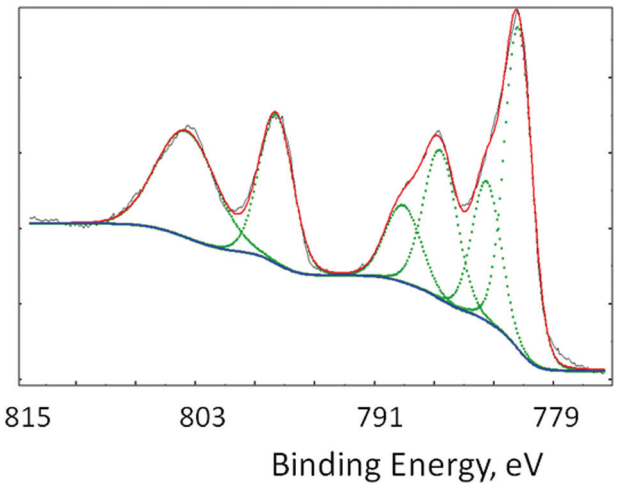

Fig. 10 Peak fitting analysis of Co 2p signals of XPS for the reference compound $CoCl_2$.

Table 4 Al $2p_{3/2}$ spectral fitting parameters: binding energy (eV) and percentage of total area[a] of the samples Co–Z-2.1-ac and Al–Co–Z-2.1-ac

Compound	Co–Z-2.1-ac	Al–Co–Z-2.1-ac	Al–Co–ZSM-5 aq[57]
Al, eV (%)	74.7	74.7 (66%) 75.7 (34%)	74.5

[a] Fitting for Al–Co–Z-ac was realized assuming fitting parameters (binding energy (eV) and FWHM) that were found for the spectrum of Co–Z-ac.

Table 5 Catalyst composition evaluated from XPS data of the samples Co–Z-2.1-ac and Al–Co–Z-2.1-ac in comparison with data from ICP analysis

	100·Co/Si, mol		Si/Al, mol		Co/Al, mol	
Sample	ICP	XPS	ICP	XPS	ICP	XPS
Co–Z-2.1-ac	3.1	4.6	23.2	22.1	0.62	1.02
Al–Co–Z-2.1-ac	3.1	6.6	9	3.6	0.28	0.24

very strong) bonds between cobalt and chlorine atoms in the last case.

The parameters of the Al $2p_{3/2}$ photoemission spectra for the samples Co–Z-2.1-ac and Al–Co–Z-2.1-ac are reported in Table 4. It can be seen that the electronic state of aluminum also changes after treatment of the parent support with anhydrous aluminum chloride. In additional to the initial aluminum located predominantly in the zeolite framework (BE of Al $2p_{3/2}$ is 74.5 eV), a new state of Al with a higher BE of Al $2p_{3/2}$ (at 75.4 eV) came into view on the surface of the modified zeolite (see Table 4). It should be noted that similar treatment of the zeolite with water aluminum salts does not change the BE of Al $2p_{3/2}$,[57] although the simultaneous presence of $Al^{3+}$and Co^{2+} in the wash-coating suspension can lead to the generation a new $Co_{1+y}Al_{2-x}O_4$ spinel species.

Table 5 gives the content of elements on the surface of two samples (Co–Z and Al–Co–Z) evaluated from their respective XPS spectra. The Si/Al ratios of Co–Z-2.1-ac obtained from the XPS spectra are similar to those obtained from ICP analysis, but according to XPS the Co/Si and Co/Al ratios for this sample are about 1.5 times higher. Higher values for Co content on the surface of the sample Co–Z-2.1-ac indicate the formation of extralattice cobalt oxides, probably located on or near the surface of the zeolite grains. This is in good agreement with the above XPS spectra (Fig. 9(A) and Table 3) and XAS data revealing the presence of Co oxide (most probably Co_3O_4 and CoO), even in the Co–Z-0.9 samples with low cobalt contents.

Table 5 also shows that the Si/Al ratio from the XPS data of the sample Al–Co–Z-2.1-ac is about 3 times smaller than that obtained from ICP. It provides support for our idea that the immobilization of $AlCl_3$ mainly proceeds in accordance with reaction (1) on the zeolite surface.

The Co/Si ratio calculated from XPS data for Al–Co–Z-2.1-ac is higher than that obtained from the chemical analysis, and this may be due to the presence of extralattice cobalt oxides or other species. Moreover the Co/Al ratio on the surface of the Al–Co–Z-2.1-ac calculated from XPS data in contrast to the Co–Z-2.1-ac sample is close to the Co/Al ratio in the entire volume of Al–Co–Z-2.1-ac (see Table 5). This may be due to the interactions between cobalt and aluminum atoms that are located close to each other on the zeolite surface, and are probably bonded through bridging the chlorine atom of extraframework $AlCl_x$ (where x = 1, 2). This assumption is in agreement with

the above Co $2p_{3/2}$ and Al $2p_{3/2}$ spectra (Tables 3 and 4) that indicate the new electronic states of both cobalt and aluminum in the Al–Co–Z sample.

By this means, XPS and XAS studies allow us to conclude that the new Co states are produced resulting from the treatment of Co-modified zeolite with anhydrous aluminum chloride. The appearance of this new type of Co coordination affects the adsorption properties of Al–Co–Z with respect to CO and C_2H_6 molecules.

Apparently, the occurrence of chlorine in the immediate environment of the cobalt ions is due to its coordination with the immobilized aluminum chloride. One can imagine several possible methods for such binding. It is known[5,23,26] that cobalt cations are exchanged not only with bridging protons in zeolite channels, but also with acidic protons located on the outer surface of crystallites, on structural defects, or in transport pores of the zeolite. The extraframework Al atoms in the fragments can bind to silicon atoms or be exchanged for bridging protons in the channels as well. The presence of extraframework aluminum of (–O–)$AlCl_x$ fragments on the Al–Co–ZSM-5 surface in the immediate vicinity of Co ions can lead to the formation of Co–Cl–Al fragments similar to the Fe–O–Al structures.[41] The halogen bridges are the basic structural elements of numerous complexes and association species formed by chlorides of these metals.[16,17,52]

Furthermore, a decrease (in accordance with X-ray diffraction and spectroscopy) of the proportion of the mixed oxide phase Co_3O_4 on the surface of Co–ZSM-5 after immobilization of aluminum chloride and the appearance of chlorine atoms in the vicinity of the cobalt atoms instead of the oxygen atoms also demonstrate the possibility of forming Co–Cl–Al structures on the surface of the zeolite that are similar to cobalt halide–aluminum chloride complexes identified in the gas phase[52] and observed at low temperatures.[15,16] It was proposed that alkane reforming catalyzed by Al–Co–ZSM-5 may take place on these sites[5] or on cluster structures containing cobalt–cobalt links formed from nearby Co–Cl–Al fragments. According to DFT calculations[58,59] bimetallic alkyl clusters containing Co–Co dimeric bonds are key intermediates leading to the formation of both isomerization products and products of alkane metathesis. The sequence of mutual rearrangement of the polynuclear complexes involving metal–carbon bond formation provides a possibility for cleavage and formation of C–C bonds in alkanes. In this connection, the modification of the zeolite both by transition metal and strong Lewis acid (anhydrous $AlCl_3$) seems quite promising for the development of new catalysts for alkane activation.

Conclusions

In accordance with DRIFT spectral studies of adsorbed probe molecules (carbon monoxide, ethane), X-ray absorption spectroscopy and XPS data, the treatment of Co–ZSM-5 with anhydrous $AlCl_3$ gives rise to the formation of a new electronic state of cobalt bonded with surface aluminum atoms through chlorine or oxygen atoms. This unusual Co coordination state on the surface of Al–Co–ZSM-5 is associated with a new band of adsorbed CO at 2192 cm^{-1}, shifted to lower frequencies compared to the complexes of CO with isolated ions Co^{n+} (2205 cm^{-1}). According to the spectral data for ethane adsorption, the specific centers of alkane activation – coordinately unsaturated cobalt ions – also changed after treatment of the surface of the Co-containing zeolite with aluminum chloride. In accordance with EXAFS, XANES and XPS data, only oxygen atoms surrounded cobalt in the samples of Co–Z prepared by using both cobalt acetate and chloride as precursors. However, after the immobilization of aluminum chloride on the surface of the zeolite Co–Z, chlorine atoms appear in the immediate vicinity of cobalt. The appearance of new states of the transition metal in modified Al–Co–ZSM-5 can be associated with a direct interaction between immobilized aluminum chloride and cobalt ions both in exchange positions and oxide-like species. It is likely that new compounds similar to cobalt halide–aluminum chloride complexes identified in the gas phase and observed at low temperatures are produced. According to our calculation for such bimetallic systems,[58,59] the transition metal cation that interacts with alkanes forming alkyl–metal derivatives plays a key role in alkane activation *via* metal alkyl intermediates. These results provide new important information for the rational design of more efficient and selective catalysts based on metal-modified zeolites for hydrocarbon conversion.

Acknowledgements

We are grateful to E. A. Nesterova and K. I. Maslakov (Research and Education Center of Collective Use of MSU Chemistry Department) for their assistance in XPS studies. This work was supported by the Russian Foundation for Basic Research, project no. 12-03-00595.

References

1 V. B. Kazansky, A. I. Serykh and E. A. Pidko, *J. Catal.*, 2004, **225**, 369.
2 Y. G. Kolyagin, V. V. Ordomsky, Y. Z. Khimyak, A. I. Rebrov, F. Fajula and I. I. Ivanova, *J. Catal.*, 2006, **238**, 122.
3 P. B. Armentrout, *Organometallics*, 2007, **26**, 5486.
4 C. Hall and R. N. Perutz, *Chem. Rev.*, 1996, **96**, 3125.
5 M. I. Shilina, O. V. Udalova and S. M. Nevskaya, *Kinet. Catal.*, 2013, **54**, 691.
6 Y. Ono, T. Tanabeand and N. Kitajima, *J. Catal.*, 1979, **56**, 47.
7 M. Sasaki, C. Songand and M. A. Plummer, *Fuel*, 2000, **79**, 295.
8 N. R. Bursian, S. B. Kogan, D. S. Orlov and E. I. Zhemchugova, *Zh. Prikl. Khim.*, 1986, **59**, 1570.
9 M. F. Polubentseva, V. V. Duganova and G. A. Mikhailenko, *Zh. Obshch. Khim.*, 1996, **66**, 630.

10 G. Olah, O. Faroog and G. K. S. Prakash, in *Activation and Functionalization of Alkanes*, ed. C. Hill, Wiley, New York, 1989.
11 Y. Ono, *Catal. Today*, 2003, **81**, 3.
12 V. M. Akhmedov and S. H. Alkhowaiter, *Catal. Rev. Sci. Eng.*, 2007, **49**, 33.
13 O. V. Krylov, *Geterogennyi kataliz (Heterogeneous Catalysis)*, Akademkniga, Moscow, 2004.
14 M. I. Shilina, R. V. Bakharev and V. V. Smirnov, *Dokl. Phys. Chem.*, 2005, **401**, 63.
15 M. I. Shilina, R. V. Bakharev, G. M. Kuramshina and V. V. Smirnov, *Russ. Chem. Bull.*, 2004, **53**, 297.
16 M. I. Shilina, R. V. Bakharev and V. V. Smirnov, *Russ. Chem. Bull.*, 2008, **57**, 2251.
17 I. P. Gloriozov, G. M. Zhidomirov and M. I. Shilina, *Russ. Chem. Bull.*, 2010, **59**, 1871.
18 M. I. Shilina, V. V. Smirnov and R. V. Bakharev, *Russ. Chem. Bull.*, 2010, **59**, 1119.
19 A. A. Chernyshov, A. A. Veligzhanin and Y. V. Zubavichus, *Nucl. Instrum. Methods Phys. Res., Sect. A*, 2009, **603**, 95.
20 PDF-2 Data Base (Sets 1–47), 1997, JCPDS – International Centre for Diffraction Data.
21 B. Ravel and M. Newville, *J. Synchrotron Radiat.*, 2005, **12**, 537.
22 A. L. Ankudinov, B. Ravel, J. J. Rehr and S. D. Conradson, *Phys. Rev. B: Condens. Matter*, 1998, **58**, 7565.
23 E. A. Paukshtis, *IK-spektroskopiya v geterogennom kislotno-osnovnom katalize (IR Spectroscopy Applied to Heterogeneous Acid–Base Catalysis)*, Nauka, Novosibirsk, 1992.
24 A. Davydov, *Molecular Spectroscopy of Oxide Catalyst Surfaces*, John Wiley & Sons Ltd, Chichester, England, 2003, pp. 1–668.
25 J. Weitkamp and M. Hunger, *Stud. Surf. Sci. Catal.*, 2007, **168**, 787.
26 T. Montanari, O. Marie, M. Daturi and G. Busca, *Catal. Today*, 2005, **110**, 339.
27 P. Hoffmann and J. A. Lobo, *Microporous Mesoporous Mater.*, 2007, **106**, 122.
28 E. Loeffler, U. Lohse, C. Peuker, G. Oehlmann, L. M. Kustov, V. L. Zholobenko and V. B. Kazansky, *Appl. Spectrosc.*, 1990, **10**, 266.
29 M. E. Malyshev, E. A. Paukshtis, L. V. Malysheva, A. V. Toktarev and L. A. Vostrikova, *Kinet. Catal.*, 2005, **46**, 107.
30 K. Hadjiivanov, *Adv. Catal.*, 2014, **57**, 99.
31 T. Xu, N. Kob, R. S. Drago, J. B. Nicholas and J. F. Haw, *J. Am. Chem. Soc.*, 1997, **119**, 12231.
32 G. Catana, D. Baetens, T. Mommaerts, R. A. Schoonheydt and B. M. Weckhuysen, *J. Phys. Chem. B*, 2001, **105**, 4904.
33 T. Montanari, O. Marie, M. Daturi and G. Busca, *Appl. Catal., B*, 2007, **71**, 216.
34 K. Gora-Marek, B. Gil, M. Sliwaand and J. Datka, *Appl. Catal., A*, 2007, **330**, 33.
35 M. Mhamdi, S. Khaddar-Zine and A. Ghorbel, *Appl. Catal., A*, 2009, **357**, 42.
36 K. Charakova and K. Hadjiivanov, *Microporous Mesoporous Mater.*, 2009, **123**, 123.
37 K. Gora-Marek, B. Gil and J. Datka, *Appl. Catal., A*, 2009, **353**, 117.
38 G. Busca, R. Guidetti and V. Lorenzelli, *J. Chem. Soc., Faraday Trans.*, 1990, **86**, 989.
39 K. Hadjiivanov, B. Tsyntsarski, T. Venkov, D. Klissurski, M. Daturi, J. Saussey and J.-C. Lavalle, *Phys. Chem. Chem. Phys.*, 2003, **5**, 1695.
40 V. Indovina, M. C. Campa and D. Pietrogiacomi, *J. Phys. Chem. C*, 2008, **112**, 5093.
41 E. J. M. Hensen, Q. Zhu and R. A. van Santen, *J. Catal.*, 2003, **220**, 260.
42 I. R. Subbotina, V. B. Kazansky, J. Krohnert and F. C. Jentoft, *J. Phys. Chem. A*, 2009, **113**, 839.
43 V. B. Kazansky and E. A. Pidko, *J. Phys. Chem. B*, 2005, **109**, 2103.
44 G. Herzberg, *Molecular Spectra and Molecular Structure II. Infrared and Raman Spectra of Polyatomic Molecules*, ed. D. van Nostrand, New York, 1947, p. 344.
45 M. Mhamdi, S. Khaddar-Zine and A. Ghorbel, *Appl. Catal., A*, 2008, **337**, 39.
46 S. Bordiga, E. Groppo, G. Agostini, J. A. van Bokhoven and C. Lamberti, *Chem. Rev.*, 2013, **113**, 1736.
47 A. Hagen and J. Östby, Proceedings (cd-rom). ed./U. Bossel. Oberrohrdorf: European Fuel Cell Forum, 2006.
48 H. Ben Boubaker, M. Mhamdi, E. Marceau, S. Khaddar-Zine, A. Ghorbel, M. Che, Y. Ben Taarit and F. Villain, *Microporous Mesoporous Mater.*, 2006, **93**, 62.
49 C. Franch-Marti, C. Alonso-Escobar, J. L. Jorda, I. Peral, J. Hernandez-Fenollosa, A. Corma, A. E. Palomares, F. Rey and G. Guilera, *J. Catal.*, 2012, **295**, 22.
50 L. Drozdova, R. Prins, J. Dececek, Z. Sobalik and B. Wichterlova, *J. Phys. Chem. B*, 2002, **106**, 2240.
51 J.-H. Park, C. H. Park and I.-S. Nam, *Appl. Catal., A*, 2004, **277**, 271.
52 M. Hargittai, *Coord. Chem. Rev.*, 1988, **91**, 35.
53 M. C. Biesingera, B. P. Payne, A. P. Grosvenord, L. W. M. Laua, A. R. Gersonb and R. S. C. Smart, *Appl. Surf. Sci.*, 2011, **257**, 2717.
54 C. Chupin, A. C. van Veen, M. Konduru, J. Deprés and C. Mirodatos, *J. Catal.*, 2006, **241**, 103.
55 L. Gutierrez and E. A. Lombardo, *Appl. Catal., A*, 2009, **360**, 107.
56 F. Lonyi, H. E. Solt, Z. Pasztiand and J. Valyon, *Appl. Catal., B*, 2014, **150–151**, 218.
57 A. V. Boix, E. E. Miró, E. A. Lombardo and J. L. G. Fierro, *Catal. Today*, 2008, **133–135**, 428.
58 M. I. Shilina, I. P. Gloriozov and G. M. Zhidomirov, *Russ. Chem. Bull.*, 2012, **61**, 1850.
59 M. I. Shilina, I. P. Gloriozov and G. M. Zhidomirov, *Russ. Chem. Bull.*, 2013, **62**, 2093.